
On-Chip Optical Transduction Scheme for Graphene Nano-Electro-Mechanical Systems in Silicon-Photonic Platform

Aneesh Dash¹, S.K. Selvaraja^{1,**}, A.K. Naik^{1,*}

1 Centre for Nano Science and Engineering, Indian Institute of Science, Bangalore

*** Corresponding author: anaik@iisc.ac.in**

**** Corresponding author: shankarks@iisc.ac.in**

Abstract

We present a scheme for on-chip optical transduction of strain and displacement of Graphene-based Nano-Electro-Mechanical Systems (NEMS). A detailed numerical study on the feasibility of three silicon-photonic integrated circuit configurations is presented: Mach-Zehnder Interferometer (MZI), micro-ring resonator and ring-loaded MZI. An index-sensing based technique using an MZI loaded with a ring resonator with a moderate Q-factor of 2400 can yield a sensitivity of $28 fm/\sqrt{Hz}$, and $6.5 \times 10^{-6}\%/ \sqrt{Hz}$ for displacement and strain respectively. Though any phase-sensitive integrated-photonic device could be used for optical transduction, here we show that optimal sensitivity is achievable by combining resonance with phase-sensitivity.

Graphene-based NEMS devices have attracted a wide range of research-interest due to ultra-low mass-density and tunability of electrical and mechanical properties [1–6]. These devices hold promise for ultra-low mass-sensing [7, 8], force-sensing [9], charge-sensing [10], and to study non-linear dynamics. Electrical transduction schemes [11] are the predominant method for transducing the motion of these devices. These methods rely on the modulation of conductance of graphene during vibration of the device. The transduction is realized either by a direct measurement scheme [12] at the frequency of vibration or by a frequency-mixed-down technique [1]. However, the presence of a large background signal and small Signal-to-Noise Ratio (SNR) make the implementation of this scheme challenging. Furthermore, the displacement sensitivities obtained with electrical transduction are generally insufficient to observe the thermo-mechanical noise [13].

Optical transduction techniques offer better displacement sensitivities (in fm/\sqrt{Hz}), large bandwidths, and signal with minimal background [14]. However, most existing optical measurement schemes are based on free-space optics, where the set-up is large and requires precise alignment of optical components [15, 16]. Integrated optics has been used for transduction of these devices, but the NEMS and optics are fabricated on different substrates and hence the challenge of alignment persists [17]. A completely integrated optical transduction scheme would help overcome such challenges.

Recent reports on graphene-based nano-photonic modulators explore the prospect of integrating graphene on a silicon-photonic platform for electro-optic applications at Near-IR wavelengths [18, 19]. Similar integration of graphene-based NEMS devices can

allow for transduction by index-based sensing, which is a well-established field in silicon photonics [20–23]. Complex refractive index-based sensing allows us to capture both dispersive and dissipative effects of graphene at Near-IR wavelengths [17, 19]. Hence, we choose it over purely reflection-based, refraction-based, or absorption-based sensing. Besides displacement, another important property to be measured in these NEMS devices is the static strain, which sets the linear dynamic range of operation of these devices [24–27]. We show that index-based sensing in graphene offers a direct method for transduction of strain.

We propose a transduction scheme with integration of the graphene NEMS device on a Silicon-photonic platform, operating around a wavelength of $1550nm$, with high sensitivity to strain and displacement. We have carried out extensive simulations using a finite element model (FEM). We use the results for calculations of response to strain and displacement using MZI, ring resonator, and ring-loaded MZI. We find that the response of the ring-loaded MZI is the best of the three. We then compute sensitivity of the transduction scheme using ring-loaded MZI to strain and displacement.

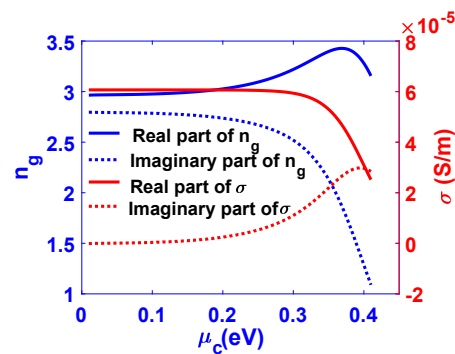


Figure 1. Refractive index n_g (left axis) and Optical conductivity σ (right axis) of graphene at $1550nm$

The in-plane refractive index of graphene and the geometry of the NEMS device over a waveguide-section determine the effective refractive index, which governs the optical response of the device. The refractive index of graphene is given by $n_g(\omega) = \sqrt{\epsilon_g(\omega)}$, where ϵ_g is the dielectric constant of graphene. For a monolayer graphene flake of thickness Δ and an optical conductivity σ as given in [28], ϵ_g is given as [29]

$$\epsilon_g(\omega) = 1 + \frac{j\sigma(\omega)}{\omega\epsilon_0\Delta}, \quad (1)$$

where ω is the optical frequency and ϵ_0 is the permittivity of free space. Both conductivity and refractive index are dependent on the chemical potential μ_c . We use it to set the operating point for measuring strain and displacement. Since the refractive index of graphene is anisotropic, we consider the out-of-plane index to be 1 [30].

Uniaxial strain ϵ in graphene leads to a change in the conductivity in the direction of strain as [31]

$$\sigma \approx \sigma_0(1 - 4\epsilon), \quad (2)$$

where σ_0 is the optical conductivity at the operating point. We neglect the anisotropic variation of conductivity with strain in the transverse direction, since we use a cross-sectional model in our analysis. The variation of n_g and σ with μ_c in this range for $1550nm$ wavelength is shown in Fig. 1. We observe that at $\mu_c = \hbar\omega/2$, which is $0.4eV$ in Fig. 1, there is sharp change in both n_g and σ . This is due to the onset of Pauli-blocking of inter-band transition in graphene. The value of $\delta n_g/\delta\sigma \approx 10^4$ at this

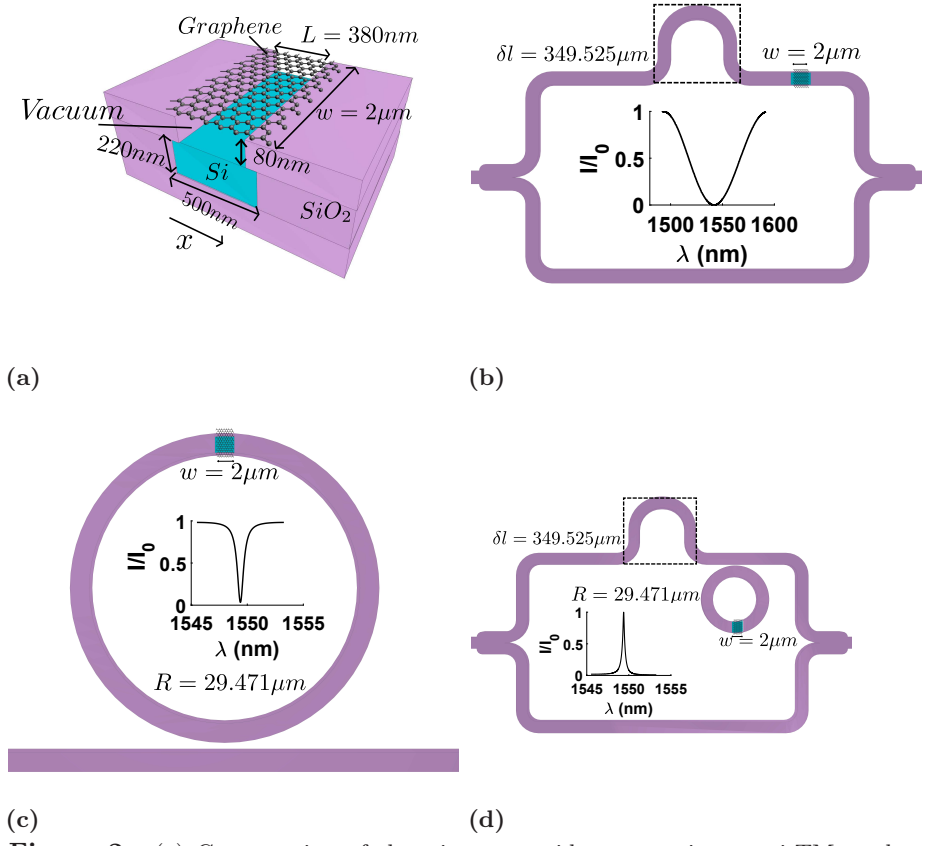
point promises good sensitivity. In addition, the real part of n_g is maximum and hence the index contrast of graphene with the core and cladding of the waveguide would be maximum at this point. Thus, the change in the effective refractive index would be dominated by the change in n_g . We, therefore, choose this as our operating point. We expect the sensitivity to strain and displacement to be maximum at this operating point. The influence of strain on the conductivity and thus the refractive index of graphene can be utilized to ascertain the applied static strain in the graphene-based NEMS devices. For calculating the response to strain, we use a flat graphene sheet over a waveguide section to compute the effective indices for different values of strain. During vibration, the dynamic strain due to change in length of graphene will produce a proportional modulation in the index of graphene. As graphene approaches and recedes from the waveguide during vibration, there will be a modulation in the effective refractive index. Thus the vibration response for the fundamental mechanical mode with resonant frequency Ω is expected to consist of a displacement component at frequency Ω and a strain component at frequency 2Ω . However, we find that this 2Ω component is not discernible in our vibration response for the dimensions of graphene considered. To calculate the displacement response, we use the mode shape of the fundamental mode for a fixed-fixed beam, which is given as [32]

$$\Phi(x) = \frac{\cosh(bx) - \cos(bx) - \sigma_m(\sinh(bx) - \sin(bx))}{\Phi_m}, \quad (3)$$

where $\Phi_m = 1.6$, $b = \sqrt{22.4}/L$, L being the length of the graphene beam, x is position along the length of the beam as shown in Fig. 2a, and $\sigma_m = [\cos(bL) - \cosh(bL)]/[\sin(bL) - \sinh(bL)]$. The time-varying displacement at mechanical resonance is given by $A\Phi(x)\cos(\Omega t)$, where A is the amplitude of vibration. We obtain the effective indices by using this mode-shape of graphene, instead of a flat graphene sheet at different phases of vibration. This is because the interaction between graphene and the optical mode in the waveguide varies as a function of x and using a flat graphene sheet would overestimate the interaction. We present the results for a moderate vibration amplitude of $100pm$ [1].

The cross-section of the wire waveguide with suspended graphene, used for computing effective indices is shown in Fig. 2a. We use a waveguide cross-section of $500nm \times 220nm$ with oxide side-clad, supporting the quasi-TM mode. We have chosen the quasi-TM mode over the quasi-TE mode because the former has greater modal overlap with the suspended graphene. This is because it has large components of electric field both perpendicular to graphene and along the direction of propagation, due to the high index-contrast of the Si core with the cladding, and thus shows a larger change in effective index. We use both the real (n_{effg}) and imaginary (k_{effg}) parts of the effective index in our calculations to capture both electro-refractive and electro-absorptive effects in graphene. Typical values obtained from our simulations are $n_{effg} = 1.61$ and $k_{effg} = 0.89 \times 10^{-3}$. Our bandwidth of operation is from $1550nm$ to $1570nm$. Since we use a single wavelength in our calculations, we ignore waveguide-dispersion in this band. For the length-scales we have considered, the loss in the waveguide-section with graphene and the loss along the ring dominate over the propagation loss along Si waveguides, and hence it is neglected [33].

The TM-waveguide cross-section with suspended graphene of length $w = 2\mu m$ forms a small part of an MZI, a micro-ring resonator, and a ring-loaded MZI. The MZI has a phase-sensitive intensity response. The micro-ring resonator is a resonant device and hence has a sharp phase transition at resonance. The MZI loaded with a ring leverages upon the phase response of the ring and the intensity response of the MZI. A schematic of the unbalanced MZI, with suspended graphene on the longer arm, is shown in Fig. 2b. For MZI without graphene, destructive interference is observed at



(a) Cross-section of the wire waveguide, supporting quasi-TM mode, with suspended graphene (b) Schematic of MZI with graphene: inset shows normalized intensity response with graphene, (c) Schematic of Ring resonator with graphene: inset shows normalized transmission response with graphene, (d) Schematic of Ring-loaded MZI with graphene: inset shows the normalized intensity response with graphene which has the smallest full-width at half-maximum (FWHM) of the three.

wavelength $\lambda_{int0} = \delta l / (m - 1/2)$, where δl is the optical path difference between the two arms without graphene and m is an integer corresponding to the number of the dark fringe. The wavelength of destructive interference for an identical MZI with graphene $\lambda_{int} = [\delta l + (n_{effg} - n_{eff0})w] / (m - 1/2)$, where n_{eff0} is the effective index in the absence of graphene. We have chosen δl such that there is a dark fringe at $1550nm$ in the absence of graphene. The transmitted intensity with graphene, assuming an amplitude splitting of 50% in both arms for an input intensity of I_0 , is given as,

$$I = I_1 + I_2 + 2\sqrt{I_1 I_2} \cos(\Delta\phi), \quad (4)$$

where $\Delta\phi = (2\pi/\lambda)[\delta l + (n_{effg} - n_{eff0})w]$, n_{eff0} the effective index of the waveguide section without graphene, $I_1 = I_0/4 \cdot \exp(-4\pi k_{effg}w/\lambda)$, and $I_2 = I_0/4$. The normalized intensity response for $w = 2\mu m$ is shown in the inset of Fig. 2b.

In a micro-ring resonator, the resonant electric field gets enhanced and hence, graphene interacts with a stronger electric field [34]. The ring resonator with graphene is shown in Fig. 2c. The resonant wavelength of the ring resonator without graphene $\lambda_{res0} = n_{eff0}(2\pi R)/n$, where R is the radius of the ring and n is the number of the resonant mode. For a ring with self-coupling coefficient r and amplitude coefficient a , the field-enhancement factor is given by $FE = \sqrt{\sqrt{ra}/(1-ra)}$, as defined in [34,35]. The electric field, enhanced by a factor FE , induces a surface current $J = \sigma FE$ in graphene. We account for this surface current by replacing σ with σFE in Eq. 1 and re-computing the corresponding values of n_g and n_{effg} for the quasi-TM mode. The ring we have used has $R = 29.47\mu m$ and $\lambda_{res0} = 1550nm$. The attenuation along the ring is $\approx 10.6dB/cm$, quality factor is ≈ 2400 , and $FE = 1.9$. For suspended graphene covering a length w along the ring, the modified resonant wavelength $\lambda_{res} = [n_{eff0}(2\pi R - w) + n_{effg}(w)]/m$.

The transmission response with graphene at the through-port, for an input intensity I_0 , is given by

$$I = I_0 \frac{a_g^2 - 2ra_g \cos(\phi) + r^2}{1 - 2ra_g \cos(\phi) + (ra_g)^2}, \quad (5)$$

where ϕ is the phase detuning from resonance and the effective amplitude coefficient with graphene is given by $a_g = a^{(1-w/(2\pi R))} \cdot \exp(-2\pi k_{effg}w/\lambda)$. The normalized transmission response for $w = 2\mu m$ is shown in the inset of Fig. 2c.

The ring-loaded MZI with graphene is shown in Fig. 2d. The overall phase delay introduced by the ring resonator with graphene is [35]

$$\phi_{ring} = \pi + \theta + \arctan\left(\frac{r \sin \theta}{a_g - r \cos \theta}\right) + \arctan\left(\frac{ra_g \sin \theta}{1 - ra_g \cos \theta}\right), \quad (6)$$

where $\theta = 2\pi\lambda_{res}/FSR(\lambda/\lambda_{res} - 1)$ is the phase detuning from the resonance and $FSR = \lambda_{res0}^2/(2\pi R n_{effg})$ is the free-spectral range of the ring. The phase difference between the two arms of the modified MZI is given as $\Delta\phi_2(\lambda) = 2\pi/\lambda[\delta l + \phi_{ring}(\lambda)]$. In the absence of graphene, a bright fringe occurs at $1550nm$. With suspended graphene over the ring, we obtain the normalized intensity response for $w = 2\mu m$ using $I_1 = I_2 = I_0/4$ and $\Delta\phi_2$ instead of $\Delta\phi$ in Eq. 4. The intensity profile is shown in the inset of Fig. 2d.

We choose the optimal probe wavelength that corresponds to the maximum gradient ($0.4nm^{-1}$, $1.7nm^{-1}$, and $8.8nm^{-1}$) of the intensity response of the MZI, ring resonator, and ring-loaded MZI respectively. We get the response to applied static strain, shown in Fig. 3a. $\epsilon_{applied} = 0\%$ corresponds to the intrinsic strain. The ring-loaded MZI shows the best overall change of 1.8×10^{-4} for 0.1% applied static strain. The changes in $\Delta P/P_0$ are of the order 10^{-4} . Optical probe powers can range from a few nW to a few μW [15–17]. For a probe power of $10nW$, the above-stated changes are detectable

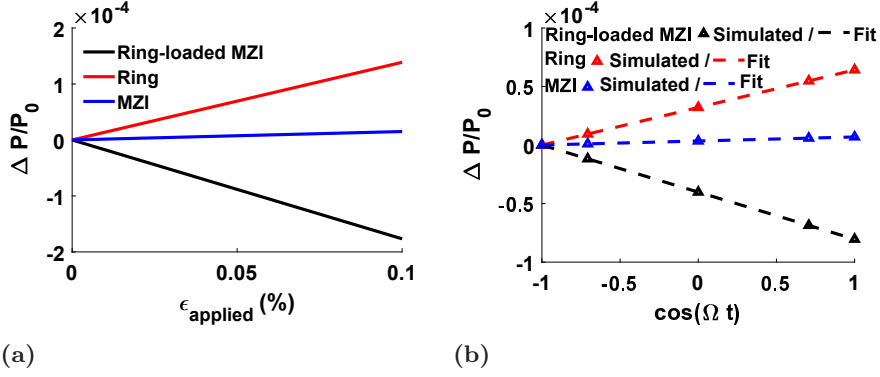


Figure 3. (a) Power response to applied static strain: Ring-loaded MZI shows an overall change of 1.8×10^{-4} which is the best of the three, (b) Power response to vibration of amplitude 100pm : Fits are of the form $y = m_1 \cos(\Omega t) + c$ indicating linearity of the response to displacement. Ring-loaded MZI shows the best overall change of 0.8×10^{-4} . Changes in n_{eff} are of the order 10^{-6}

by commercially available InGaAs photo-detectors with noise-equivalent power (NEP) of the order fW/\sqrt{Hz} with less than 1MHz measurement bandwidth. The power response to a vibration amplitude of 100pm is shown in Fig. 3b. The data-points correspond to five phases during vibration. The ring-loaded MZI shows the best overall change with vibration (0.8×10^{-4}). The responses show a linear fit to $\cos(\Omega t)$. With a probing set-up identical to that considered for static strain, changes of this order are also detectable with less than 1MHz measurement bandwidth. The noise in the responses depends on the input noise in the probe, quantified by the relative intensity noise (RIN), and the NEP of the photo-detector. We consider RIN of the probe to be limited only by the photon shot noise. The RIN is lower for higher output powers and the absolute output power in response to static strain and displacement depends on the input probe power. Thus, for measuring extremely small changes in static strain and displacement with the ring-loaded MZI configuration, we use a relatively higher input probe power of $10\mu\text{W}$. The noise spectral density at this power and wavelength is $N_s = 1.6 \times 10^{-12} \text{W}/\sqrt{Hz}$, which is greater than the NEP ($= 10^{-15} \text{W}/\sqrt{Hz}$) we have considered. So, the sensitivities are limited by the source. We extract displacement and strain sensitivities of $398.3 \text{fm}/\sqrt{Hz}$ and $9.1 \times 10^{-5} \%/ \sqrt{Hz}$ respectively for $w = 2\mu\text{m}$.

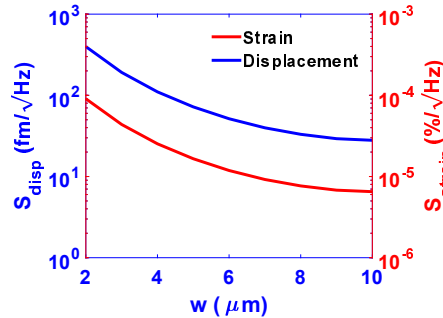


Figure 4. Sensitivity of Ring-loaded MZI to Static strain and Displacement: Best sensitivities of $6.5 \times 10^{-6} \%/ \sqrt{Hz}$ and $28 \text{fm}/\sqrt{Hz}$ respectively at $w = 10\mu\text{m}$

As we increase w , the interaction length of graphene with the ring-loaded MZI increases leading to an improvement in the sensitivities, as observed in Fig. 4. For a

gap of 80nm under graphene and $L = 380\text{nm}$, it is possible to fabricate suspended devices with w of $10\mu\text{m}$, beyond which there is a risk of collapse of graphene. For $w = 10\mu\text{m}$, we compute sensitivities of $28\text{fm}/\sqrt{\text{Hz}}$ and $6.5 \times 10^{-6}\%/\sqrt{\text{Hz}}$ for displacement and strain respectively. These notable sensitivities offer the ability to detect thermomechanical noise. The probe power of $10\mu\text{W}$ is at the input of the ring-loaded MZI. In our configuration, the power in the waveguide section under graphene would be $\approx 2.5\mu\text{W}$. For our quasi-TM mode, the power at the surface of graphene would be lower by a factor of 100. At these power levels, photothermal and optomechanical effects due to the probe laser can be ignored [17, 36, 37]. Hence this detection scheme has negligible back-action.

We have shown that the ring-loaded MZI is the best of the three silicon-photonics devices considered for measuring displacement and strain in graphene NEMS. It offers sensitivities of $28\text{fm}/\sqrt{\text{Hz}}$ and $6.5 \times 10^{-6}\%/\sqrt{\text{Hz}}$ respectively. The individual displacement and strain responses are linear. Even with a ring of moderate quality factor of 2400, such high sensitivities can be achieved. A moderate quality factor also allows for a large dynamic range of vibration amplitudes. Since this is a completely integrated index-sensing based technique, there are no challenges of precise alignments and isolation of stray reflections, as in other optical transduction schemes, while high displacement sensitivity is retained [14, 17]. Further improvement in sensitivity can be achieved by reducing the gap between graphene and the Si waveguide or by using transduction schemes with steeper intensity response [38]. The analysis here is general to any method of actuation, though each actuation scheme would have its independent effect on the output and would have to be addressed separately. This technique can be used to study thermomechanical noise and vibration-dynamics in graphene NEMS, with applications in mass-sensing, force-sensing, and charge-sensing. Thus a ring-loaded MZI holds considerable potential for a highly sensitive, completely integrated silicon-photonics platform for optical transduction in graphene NEMS.

Funding

Council of Scientific and Industrial Research (CSIR), Government of India and Ministry of Electronics and Information Technology (MeitY), Government of India.

References

1. C. Chen, S. Rosenblatt, K. I. Bolotin, W. Kalb, P. Kim, I. Kymissis, H. L. Stormer, T. F. Heinz, and J. Hone, "Performance of monolayer graphene nanomechanical resonators with electrical readout," *Nat Nano*, vol. 4, no. 12, pp. 861–867, Dec. 2009. [Online]. Available: <http://www.nature.com/nnano/journal/v4/n12/abs/nnano.2009.267.html>
2. R. A. Barton, B. Ilic, A. M. van der Zande, W. S. Whitney, P. L. McEuen, J. M. Parpia, and H. G. Craighead, "High, Size-Dependent Quality Factor in an Array of Graphene Mechanical Resonators," *Nano Lett.*, vol. 11, no. 3, pp. 1232–1236, Mar. 2011. [Online]. Available: <http://dx.doi.org/10.1021/nl1042227>
3. J. P. Mathew, R. N. Patel, A. Borah, R. Vijay, and M. M. Deshmukh, "Dynamical strong coupling and parametric amplification of mechanical modes of graphene drums," *Nat Nano*, vol. 11, no. 9, pp. 747–751, Sep. 2016. [Online]. Available: <http://www.nature.com/nnano/journal/v11/n9/full/nnano.2016.94.html>

-
4. M. M. Benameur, F. Gargiulo, S. Manzeli, G. Autès, M. Tosun, O. V. Yazyev, and A. Kis, “Electromechanical oscillations in bilayer graphene,” *Nat Commun*, vol. 6, p. 8582, Oct. 2015. [Online]. Available: <http://www.nature.com/ncomms/2015/151020/ncomms9582/full/ncomms9582.html>
 5. A. D. Smith, F. Niklaus, A. Paussa, S. Vaziri, A. C. Fischer, M. Sterner, F. Forsberg, A. Delin, D. Esseni, P. Palestri, M. Östling, and M. C. Lemme, “Electromechanical Piezoresistive Sensing in Suspended Graphene Membranes,” *Nano Lett.*, vol. 13, no. 7, pp. 3237–3242, Jul. 2013. [Online]. Available: <http://dx.doi.org/10.1021/nl401352k>
 6. S. Lee, C. Chen, V. V. Deshpande, G.-H. Lee, I. Lee, M. Lekas, A. Gondarenko, Y.-J. Yu, K. Shepard, P. Kim, and J. Hone, “Electrically integrated SU-8 clamped graphene drum resonators for strain engineering,” *Appl Phys Lett*, vol. 102, no. 15, p. 153101, Apr. 2013. [Online]. Available: <http://scitation.aip.org/content/aip/journal/apl/102/15/10.1063/1.4793302>
 7. A. K. Naik, M. S. Hanay, W. K. Hiebert, X. L. Feng, and M. L. Roukes, “Towards single-molecule nanomechanical mass spectrometry,” *Nat Nano*, vol. 4, no. 7, pp. 445–450, Jul. 2009. [Online]. Available: <http://www.nature.com/nnano/journal/v4/n7/abs/nnano.2009.152.html>
 8. J. Chaste, A. Eichler, J. Moser, G. Ceballos, R. Rurali, and A. Bachtold, “A nanomechanical mass sensor with yoctogram resolution,” *Nat Nano*, vol. 7, no. 5, pp. 301–304, May 2012. [Online]. Available: <http://www.nature.com/nnano/journal/v7/n5/full/nnano.2012.42.html>
 9. P. Weber, J. Güttinger, A. Noury, J. Vergara-Cruz, and A. Bachtold, “Force sensitivity of multilayer graphene optomechanical devices,” *Nat Commun*, vol. 7, p. ncomms12496, Aug. 2016. [Online]. Available: <https://www.nature.com/articles/ncomms12496>
 10. J. S. Bunch, A. M. v. d. Zande, S. S. Verbridge, I. W. Frank, D. M. Tanenbaum, J. M. Parpia, H. G. Craighead, and P. L. McEuen, “Electromechanical Resonators from Graphene Sheets,” *Science*, vol. 315, no. 5811, pp. 490–493, Jan. 2007. [Online]. Available: <http://science.sciencemag.org/content/315/5811/490>
 11. J. Lee and T. H. Yoon, “Self-heterodyne mixing method of two inter-mode beat frequencies for frequency stabilization of a three-mode He-Ne laser,” *AIP Advances*, vol. 2, no. 2, p. 022170, Jun. 2012. [Online]. Available: <http://scitation.aip.org/content/aip/journal/adva/2/2/10.1063/1.4733344>
 12. C. Chen, “Graphene NanoElectroMechanical Resonators and Oscillators,” Ph.D. dissertation, Columbia University Academic Commons, 2013. [Online]. Available: <https://academiccommons.columbia.edu/catalog/ac%3A156928>
 13. A. M. Vadiraj Rao, “High Frequency readout scheme for Graphene based NEMS,” Master’s thesis, TU Delft, 2012. [Online]. Available: <http://repository.tudelft.nl/islandora/object/uuid:2a160a48-9388-4950-af30-24685f221489?collection=education>
 14. A. Castellanos-Gomez, V. Singh, H. S. J. van der Zant, and G. A. Steele, “Mechanics of freely-suspended ultrathin layered materials,” *Ann. Phys. (Berlin)*, vol. 527, no. 1-2, pp. 27–44, Jan. 2015. [Online]. Available: <http://onlinelibrary.wiley.com/doi/10.1002/andp.201400153/abstract>

-
15. A. M. v. d. Zande, R. A. Barton, J. S. Alden, C. S. Ruiz-Vargas, W. S. Whitney, P. H. Q. Pham, J. Park, J. M. Parpia, H. G. Craighead, and P. L. McEuen, "Large-Scale Arrays of Single-Layer Graphene Resonators," *Nano Lett.*, vol. 10, no. 12, pp. 4869–4873, Dec. 2010. [Online]. Available: <http://dx.doi.org/10.1021/nl102713c>
 16. A. Reserbat-Plantey, K. G. Schädler, L. Gaudreau, G. Navickaite, J. Güttinger, D. Chang, C. Toninelli, A. Bachtold, and F. H. L. Koppens, "Electromechanical control of nitrogen-vacancy defect emission using graphene NEMS," *Nat Commun*, vol. 7, p. 10218, Jan. 2016. [Online]. Available: <http://www.nature.com/ncomms/2016/160108/ncomms10218/full/ncomms10218.html>
 17. R. M. Cole, G. A. Brawley, V. P. Adiga, R. De Alba, J. M. Parpia, B. Ilic, H. G. Craighead, and W. P. Bowen, "Evanescent-Field Optical Readout of Graphene Mechanical Motion at Room Temperature," *Phys. Rev. Applied*, vol. 3, no. 2, p. 024004, Feb. 2015. [Online]. Available: <http://link.aps.org/doi/10.1103/PhysRevApplied.3.024004>
 18. C. T. Phare, Y.-H. Daniel Lee, J. Cardenas, and M. Lipson, "Graphene electro-optic modulator with 30 GHz bandwidth," *Nat Photon*, vol. 9, no. 8, pp. 511–514, Aug. 2015. [Online]. Available: <http://www.nature.com/nphoton/journal/v9/n8/abs/nphoton.2015.122.html>
 19. V. Soriano, G. D. Angelis, T. Cassese, M. Midrio, M. Romagnoli, M. Mohsin, M. Otto, D. Neumaier, I. Asselberghs, J. V. Campenhout, and C. Huyghebaert, "Complex effective index in graphene-silicon waveguides," *Opt. Express, OE*, vol. 24, no. 26, pp. 29984–29993, Dec. 2016. [Online]. Available: <http://www.osapublishing.org/abstract.cfm?uri=oe-24-26-29984>
 20. P. R. Prasad, S. K. Selvaraja, and M. M. Varma, "High precision measurement of intensity peak shifts in tunable cascaded microring intensity sensors," *Opt. Lett., OL*, vol. 41, no. 14, pp. 3153–3156, Jul. 2016. [Online]. Available: <http://www.osapublishing.org/abstract.cfm?uri=ol-41-14-3153>
 21. R. J. J. v. Gulik, B. M. d. Boer, and P. J. Harmsma, "Refractive Index Sensing Using a Three-Port Interferometer and Comparison With Ring Resonators," *IEEE J Sel Top Quant*, vol. 23, no. 2, pp. 433–439, Mar. 2017.
 22. D. Yang, C. Wang, and Y. Ji, "Silicon On-Chip One-Dimensional Photonic Crystal Nanobeam Bandgap Filter Integrated With Nanobeam Cavity for Accurate Refractive Index Sensing," *IEEE Photon. J.*, vol. 8, no. 2, pp. 1–8, Apr. 2016.
 23. X. Zhang, G. Zhou, P. Shi, H. Du, T. Lin, J. Teng, and F. S. Chau, "On-chip integrated optofluidic complex refractive index sensing using silicon photonic crystal nanobeam cavities," *Opt. Lett., OL*, vol. 41, no. 6, pp. 1197–1200, Mar. 2016. [Online]. Available: <http://www.osapublishing.org/abstract.cfm?uri=ol-41-6-1197>
 24. M. M. Parmar, P. R. Y. Gangavarapu, and A. K. Naik, "Dynamic range tuning of graphene nanoresonators," *Appl Phys Lett*, vol. 107, no. 11, p. 113108, Sep. 2015. [Online]. Available: <http://scitation.aip.org/content/aip/journal/apl/107/11/10.1063/1.4931118>
 25. M. D. Dai, C.-W. Kim, and K. Eom, "Nonlinear vibration behavior of graphene resonators and their applications in sensitive mass detection," *Nanoscale Res*

-
- Lett*, vol. 7, no. 1, p. 499, Sep. 2012. [Online]. Available: <http://www.ncbi.nlm.nih.gov/pmc/articles/PMC3462111/>
26. A. Reserbat-Plantey, L. Marty, O. Arcizet, N. Bendiab, and V. Bouchiat, “A local optical probe for measuring motion and stress in a nanoelectromechanical system,” *Nat Nano*, vol. 7, no. 3, pp. 151–155, Mar. 2012. [Online]. Available: <http://www.nature.com/nnano/journal/v7/n3/full/nnano.2011.250.html?WT.ec.id%3DNNANO-201203>
 27. C.-W. Kim, M. D. Dai, and K. Eom, “Finite-size effect on the dynamic and sensing performances of graphene resonators: the role of edge stress,” *Beilstein J Nanotechnol*, vol. 7, no. 1, pp. 685–696, May 2016. [Online]. Available: <https://www.beilstein-journals.org/bjnano/articles/7/61>
 28. V. P. Gusynin, S. G. Sharapov, and J. P. Carbotte, “Magneto-optical conductivity in graphene,” *J. Phys.: Condens. Matter*, vol. 19, no. 2, p. 026222, 2007. [Online]. Available: <http://stacks.iop.org/0953-8984/19/i=2/a=026222>
 29. S. P. Apell, G. W. Hanson, and C. Hägglund, “High optical absorption in graphene,” *arXiv:1201.3071 [physics]*, Jan. 2012, arXiv: 1201.3071. [Online]. Available: <http://arxiv.org/abs/1201.3071>
 30. Z. Chang and K. S. Chiang, “Experimental verification of optical models of graphene with multimode slab waveguides,” *Opt. Lett., OL*, vol. 41, no. 9, pp. 2129–2132, May 2016. [Online]. Available: <https://www.osapublishing.org/abstract.cfm?uri=ol-41-9-2129>
 31. V. M. Pereira, R. M. Ribeiro, N. M. R. Peres, and A. H. C. Neto, “Optical properties of strained graphene,” *EPL*, vol. 92, no. 6, p. 67001, 2010. [Online]. Available: <http://stacks.iop.org/0295-5075/92/i=6/a=67001>
 32. W. Thomson, *Theory of vibration with applications*. Prentice-Hall, 1988. [Online]. Available: <https://books.google.co.in/books?id=BIxRAAAAMAAJ>
 33. Y. A. Vlasov and S. J. McNab, “Losses in single-mode silicon-on-insulator strip waveguides and bends,” *Opt. Express, OE*, vol. 12, no. 8, pp. 1622–1631, Apr. 2004. [Online]. Available: <https://www.osapublishing.org/abstract.cfm?uri=oe-12-8-1622>
 34. H. Cai, Y. Cheng, H. Zhang, Q. Huang, J. Xia, R. Barille, and Y. Wang, “Enhanced linear absorption coefficient of in-plane monolayer graphene on a silicon microring resonator,” *Opt. Express, OE*, vol. 24, no. 21, pp. 24105–24116, Oct. 2016. [Online]. Available: <http://www.osapublishing.org/abstract.cfm?uri=oe-24-21-24105>
 35. W. Bogaerts, P. De Heyn, T. Van Vaerenbergh, K. De Vos, S. Kumar Selvaraja, T. Claes, P. Dumon, P. Bienstman, D. Van Thourhout, and R. Baets, “Silicon microring resonators,” *Laser & Photonics Reviews*, vol. 6, no. 1, pp. 47–73, Jan. 2012. [Online]. Available: <http://onlinelibrary.wiley.com/doi/10.1002/lpor.201100017/abstract>
 36. R. A. Barton, I. R. Storch, V. P. Adiga, R. Sakakibara, B. R. Cipriany, B. Ilic, S. P. Wang, P. Ong, P. L. McEuen, J. M. Parpia, and H. G. Craighead, “Photothermal Self-Oscillation and Laser Cooling of Graphene Optomechanical Systems,” *Nano Lett.*, vol. 12, no. 9, pp. 4681–4686, Sep. 2012. [Online]. Available: <http://dx.doi.org/10.1021/nl302036x>
-

-
37. M. Li, W. H. P. Pernice, C. Xiong, T. Baehr-Jones, M. Hochberg, and H. X. Tang, "Harnessing optical forces in integrated photonic circuits," *Nature*, vol. 456, no. 7221, pp. 480–484, Nov. 2008. [Online]. Available: <http://www.nature.com/nature/journal/v456/n7221/full/nature07545.html>
 38. C. Porzi, G. Serafino, P. Velha, P. Ghelfi, and A. Bogoni, "Integrated SOI High-Order Phase-Shifted Bragg Grating for Microwave Photonics Signal Processing," *J. Lightwave Technol.*, vol. 35, no. 20, pp. 4479–4487, Oct. 2017.